Computers and Electronics in Agriculture 68 (2009) 44–51

Contents lists available at ScienceDirect

Computers and Electronics in Agriculture

journal homepage: www.elsevier.com/locate/compag

Monte Carlo simulation for quantification of light transport features in apples

Jianwei Qin [a,*], Renfu Lu [b]

[a] Department of Biosystems and Agricultural Engineering, Michigan State University, East Lansing, MI 48824, USA
[b] Sugarbeet and Bean Research Unit, Agricultural Research Service, United States Department of Agriculture, 224 Farrall Hall, Michigan State University, East Lansing, MI 48824, USA

ARTICLE INFO

Article history:
Received 18 November 2008
Received in revised form 21 April 2009
Accepted 21 April 2009

Keywords:
Hyperspectral imaging
Optical properties
Fruits
Light transport
Monte Carlo simulation

ABSTRACT

Light interaction with turbid biological materials involves absorption and scattering. Quantitative understanding of light transport process and features in the fruit is critical to designing better optical systems for inspection of food quality. This paper reports on the quantification of light transport in the apple fruit in the visible and short-wavelength near-infrared region using Monte Carlo simulations. The absorption and reduced scattering coefficients (μ_a and μ_s', respectively) of 600 'Golden Delicious' apples were determined over the spectral range of 500–1000 nm using a spatially resolved hyperspectral imaging method coupled with a diffusion theory model. The μ_a and μ_s' values were used in Monte Carlo (MC) models to simulate light transport in the fruit tissue. MC simulation models were validated against the diffusion theory model and experimental data. The patterns of diffuse reflectance, internal absorption, and light penetration depth were determined using typical values of μ_a and μ_s' for the apples. Simulation results showed that up to 96.4% of the photons were absorbed under the maximum absorption condition, while 75.9% photons exited as diffuse reflectance for the maximum scattering case. The optimum sensing range under our imaging system setup was found to be 1–11 mm for 'Golden Delicious' apples. Fruit tissue with a larger μ_a value absorbed light energy rapidly in short depth and radial distances, whereas light in the tissue with small μ_s' values tended to propagate forward to the deeper area of the sample. Light penetration depths in 'Golden Delicious' apples, defined as the depths at which the incident light was reduced by 99%, were in the range of 0.43–8.67 cm over the 500–1000 nm spectral range, with a majority of the samples (approximately 68%) in the range of 0.81–4.48 cm. Pigments and water in the fruit tissue greatly influenced light penetration depth.

1. Introduction

Optical properties of biological materials are characterized by absorption coefficient (μ_a) and reduced scattering coefficient (μ_s'). With the knowledge of absorption and reduced scattering coefficients, we can quantitatively analyze light transport features inside intact food items (e.g., penetration depth, diffuse reflectance, and internal absorption), which are often difficult to measure experimentally. This can help us design a more effective measurement configuration (e.g., source intensity, detector position and sensing area) for different types of samples without extensive experimental tests.

Despite the wide use of light-based techniques, methods for measurement of the optical properties of food and agricultural products are still not well developed, and relevant data are largely absent in the literature. Cubeddu et al. (2001) reported on using time-resolved spectroscopy for determining the optical properties of fruits. Saeys et al. (2008) used single integrating sphere combined with inverse adding-doubling method to measure the optical properties of apple skin and flesh in the wavelength range from 350 to 2200 nm. We recently developed a novel spatially resolved method based on hyperspectral imaging for measuring the optical properties of liquid foods (e.g., milk and juice), and fruits and vegetables (Qin and Lu, 2007, 2008). Compared to time-resolved technique, the hyperspectral imaging technique is noncontact, faster and simpler for measuring the optical properties, and it is especially suitable for food and agricultural products.

Light transport in turbid media may be described by radiation transfer theory. When scattering is dominant ($\mu_s' \gg \mu_a$), the radiation transfer theory may be approximated by diffusion theory model. However, due to the complexity of the problem, one often has to use numerical or statistical methods to solve the diffusion theory model. Different methods are being used for modeling light transport in a turbid medium, of which the Monte Carlo simulation method is the most widely used. The Monte Carlo method creates a stochastic numerical model in which the expected value of a certain random variable is equivalent to the value of a physical quantity to be determined. This expected value is determined by averaging

* *Corresponding author*. Current address: Department of Agricultural and Biological Engineering, University of Florida, 233 Frazier Rogers Hall, P.O. Box 110570, Gainesville, FL 32611-0570, USA. Tel.: +1 352 392 1864x233.
E-mail address: qinj@ufl.edu (J. Qin).

0168-1699/$ – see front matter © 2009 Elsevier B.V. All rights reserved.
doi:10.1016/j.compag.2009.04.002

numerous independent samples that represent the random variable in the model. Monte Carlo simulation offers a flexible and accurate approach for investigating and understanding light transport in turbid materials, and it is particularly useful for determining the features of light transport that are difficult to measure, such as light penetration depth and the pathlength of photons that travel in the tissue. In Monte Carlo light transport simulation, a photon is injected into a turbid medium, and it then propagates through the medium, which depends on the optical properties (i.e., μ_a and μ_s') of the investigated material. The Monte Carlo method defines local rules for photon propagation that are expressed as probability distributions for describing the step size of photon movement between sites of photon–tissue interaction, and the angles of deflection in a photon's trajectory when a scattering event occurs (Wang et al., 1995). Light transport is then simulated by tracking millions of photons, and multiple physical quantities, such as diffuse reflectance and internal photon absorption, are scored simultaneously. Forward and inverse Monte Carlo models have been used for simulating light distribution in tissues (Okada et al., 1997; Wang and Liang, 1999; Tsai et al., 2001) and measuring tissue optical properties (Kienle et al., 1996; Simpson et al., 1998; Palmer and Ramanujam, 2006) in various biological materials, respectively. Other numerical approaches such as finite element method based on the diffusion approximation model (Arridge et al., 1993; Deulin and L'Huillier, 2006) have also been used to model light transport in turbid materials.

While considerable research has been reported on Monte Carlo simulations for understanding and quantifying light transport in biological materials, the application of this method for food and agricultural products has been largely absent until very recently (Fraser et al., 2003). This is partly due to the lack of optical property data for food products. This research was therefore aimed at the development of Monte Carlo models to simulate and quantify light transport in apple fruit tissues using the optical property data obtained with a newly developed spatially resolved hyperspectral imaging technique, which measures diffuse reflectance at different distances generated from a steady-state (or continuous-wave) light source for a specific spectral region. The specific objectives were to:

- measure the absorption and scattering properties of apples using a spatially resolved hyperspectral imaging technique (Qin and Lu, 2008);
- develop and validate Monte Carlo simulation models for apples using diffusion theory model and the optical property data;
- determine major light transport features in apples including diffuse reflectance, internal absorption, and penetration depth using Monte Carlo simulations;
- demonstrate the applications of simulated diffuse reflectance for determining the optimum sensing range for apples in using a hyperspectral imaging system.

2. Materials and methods

2.1. Apple samples

Six hundred 'Golden Delicious' apples were used in the optical property measurement experiment. These apples were harvested from the orchards at Michigan State University (MSU) Clarksville Horticultural Experiment Station in Clarksville, Michigan, and the MSU Horticultural Teaching and Research Center in Holt, Michigan in 2006. The apples were stored in a controlled atmosphere environment (2% O_2 and 3% CO_2 at 0 °C) for about 5 months prior to testing. Experiments were performed after these apples were removed from storage and had been kept at room temperature (~24 °C) for at least 15 h. The test apples had the mean Magness–Taylor firmness value of 56.7 N and the standard deviation of 12.1 N; their mean and standard deviation for soluble solids content were 10.7% and 1.4%, respectively. Because of large property variation in the 'Golden Delicious' apples, a typical range of optical property values would be also expected.

2.2. Hyperspectral image acquisition

A hyperspectral imaging system (Fig. 1) developed in the U.S. Department of Agriculture Agricultural Research Service (USDA/ARS) postharvest engineering laboratory at Michigan State University in East Lansing, Michigan was used for acquiring spatially resolved scattering images from apple samples. The imaging system mainly consisted of a light source unit, a hyperspectral imaging unit, and a sample handling unit. A detailed description of the hyperspectral imaging system and the procedures for acquiring spatially resolved spectral scattering images from intact fruit is given in Qin and Lu (2008). The hyperspectral imaging system was calibrated both spectrally and geometrically by following the procedure described in Lu and Chen (1998). In addition, a third calibration procedure called instrument response calibration was performed to correct nonuniform instrument responses of the imaging system by following the procedure described in Qin and Lu (2007).

Spatially resolved scattering images were acquired from each apple using the hyperspectral imaging system. The hyperspectral imaging system line scanned the sample 1.6 mm off the incident point to avoid signal saturation but without losing essential scattering information. It collected spatially resolved scattering images from each sample for every 1 mm horizontal displacement over a range of 9 mm (10 scans, see Fig. 1), as the sample was moving at a constant velocity (~0.6 mm/s) during the image acquisition. Individual scattering images from the sample were averaged to improve the signal to noise ratios and enhance the signal repeatability, and only average images were used for further analysis.

2.3. Radiation transfer model for light transport in turbid media

Light interaction with plant tissue, such as fruits and vegetables, is a complicated phenomenon. The radiation transport (RT) equation (also known as the Boltzmann equation) provides a fundamental description for the flow of energy or photons in a system. It has been successfully applied in various turbid media, such as oceans, atmosphere, interstellar materials, as well as human tissues. The RT equation can be deduced by considering the energy balance in a small volume of the turbid media (Ishimaru, 1978), and the time-dependent transport equation is given by

$$\frac{1}{c}\frac{\partial I(\vec{r},\vec{\Omega},t)}{\partial t} = -\vec{\Omega}\cdot\nabla I(\vec{r},\vec{\Omega},t) - (\mu_a+\mu_s)I(\vec{r},\vec{\Omega},t) + \mu_s\int_{4\pi} p(\vec{\Omega}',\vec{\Omega})I(\vec{r},\vec{\Omega}',t)d\Omega' + Q(\vec{r},\vec{\Omega},t) \quad (1)$$

where $I(\vec{r},\vec{\Omega},t)$ is the energy radiance, which represents the amount of energy flowing in the unit time within a unit solid angle in direction $\vec{\Omega}$ through an unit area at $\vec{r}$, μ_a and μ_s are the absorption and scattering coefficients [$\mu_s = \mu_s'/(1-g)$] when scattering is dominant, and g is the anisotropy factor of the medium], $p(\vec{\Omega}',\vec{\Omega})$ is the phase function, which equals the probability distribution of the scattering angle from $\vec{\Omega}$ to $\vec{\Omega}'$, $c = c_0/n$ is the velocity of light in the medium, where c_0 is the velocity of light in vacuum and n is the refractive index of the medium, and $Q(\vec{r},\vec{\Omega},t)$ describes a possible source within the medium. The first term on the right-hand side of Eq. (1) represents the net gain of photons at position $\vec{r}$ and direction $\vec{\Omega}$ due to the flow of photons. The second term represents the loss of photons at $\vec{r}$ and $\vec{\Omega}$ as a result of absorption and scattering. The

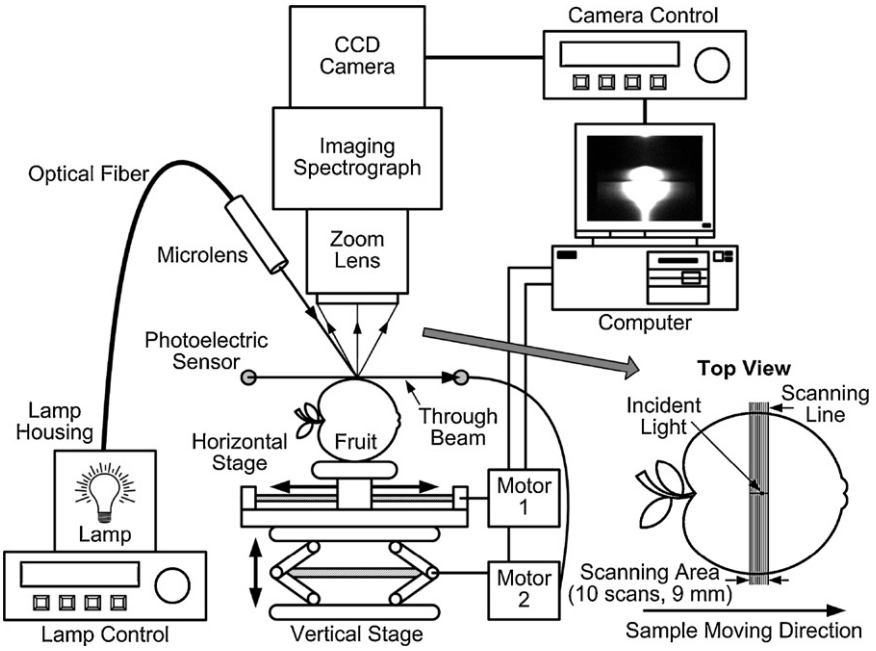

Fig. 1. Hyperspectral imaging system for acquiring spatially resolved scattering images from an apple sample.

third term represents the gain of photons at $\vec{r}$ and $\vec{\Omega}$ due to scattering. Finally, the fourth term represents the gain of photons due to the potential source.

Although the radiation transport equation forms the basis for the general treatment of light propagation in absorbing/scattering media, it is difficult to obtain direct analytical solutions to Eq. (1) for many practical problems. Most of the complications arise from dealing with the tissue boundaries and geometric aspects for samples and light sources. Thus Eq. (1) can only be solved in special cases. For example, when a steady-state (or continuous-wave) light beam is incident perpendicularly upon a semi-infinite homogeneous medium, light transport in the medium may be approximated to be a diffusion process. Farrell et al. (1992) obtained an analytical equation for predicting a spatially resolved scattering profile at the surface of the semi-infinite medium, which is dependent upon distance and absorption and reduced scattering coefficients.

2.4. Determination of the optical properties

The optical properties (μ_a and μ_s') of 'Golden Delicious' apples were determined from the spatially resolved hyperspectral images using the steady-state diffusion theory model (Farrell et al., 1992). The data analysis procedures are illustrated in Fig. 2. The original hyperspectral images were first corrected for nonuniform instrumental response. Image preprocessing, including image smoothing, was then performed to improve the signal-to-noise ratio of the corrected images. Spatially resolved diffuse reflectance profiles were extracted from the enhanced images over the wavelengths of 500–1000 nm, followed by the procedure of fruit size corrections for the spatial profiles due to the light intensity distortion caused by the curved fruit surface (Qin and Lu, 2008). The corrected spatial profiles were then normalized with respect to the peak value. Finally, the diffusion theory model was used to fit the normalized profiles using a trust-region (i.e., selecting specific ranges for unknown fitting variables) nonlinear least squares fitting algorithm to obtain the absorption and scattering spectra of the samples for the spectral region of 500–1000 nm. The procedures described above were implemented in Matlab 7.0 (MathWorks, Natick, MA, USA). The algorithm was validated by testing liquid simulation samples with different absorption backgrounds, which showed accuracies of 16% and 11% for μ_a and μ_s', respectively (Qin and Lu, 2007). A detailed description of the data analysis methods for determining the optical properties from the hyper-

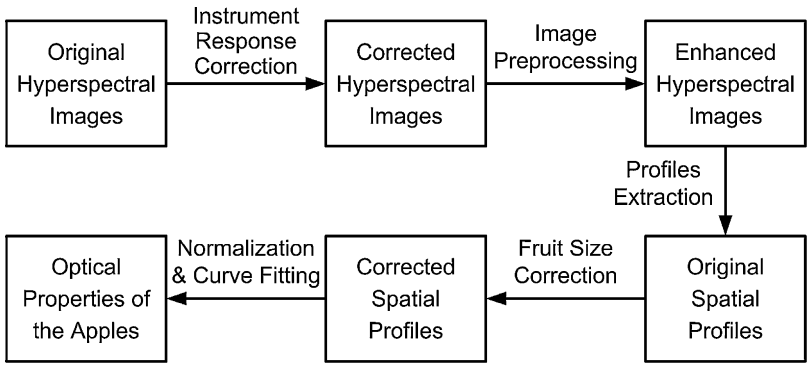

Fig. 2. Data analysis procedures for determining optical properties of apples based on hyperspectral imaging technique.

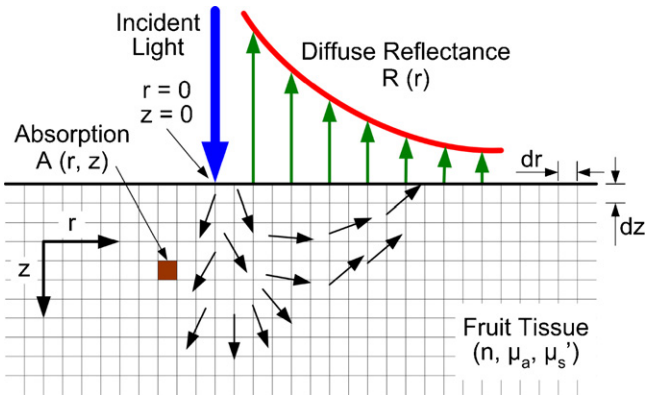

Fig. 3. Monte Carlo simulation for diffuse reflectance and internal photon absorption for an apple fruit.

spectral scattering images can be found in Qin and Lu (2007, 2008).

2.5. Monte Carlo simulation and experimental verification

Since the spatial distribution of photons inside the fruit tissue is largely confined to a small portion of the apple fruit, it was therefore reasonable to consider the fruit to be a semi-infinite turbid medium in Monte Carlo simulations. It was further assumed that apple fruit were homogeneous, although the optical properties of fruit skin are quite different from those of fruit flesh. This assumption seems justifiable given the fact that the pathlength of most photons scattering in the fruit tissue would be much greater than the thickness of apple skin (about 0.5 mm for 'Golden Delicious' apples).

Monte Carlo simulation for light diffuse reflectance and internal photon absorption in fruit tissue is illustrated in Fig. 3. After a photon packet was launched, specular reflectance from the tissue surface was immediately calculated using Fresnel equations (Bass et al., 1995), and the remaining photons were then transmitted into the fruit tissue. Some photons would exit the tissue surface and their weights were consequently scored into the diffuse reflectance array $R(r)$. On the other hand, the absorbed photon weights inside the fruit tissue were scored into the 2D absorption array $A(r, z)$, and the values in $A(r, z)$ gave the probability of photon absorption by the fruit tissue. Detailed procedures on how the weights of scattered and absorbed photons were scored into $R(r)$ and $A(r, z)$ arrays can be found in Wang et al. (1995). The simulation results obtained by the methods described above are based on the assumption that the light source is an infinitely narrow photon beam. To improve simulation accuracies, the light source profile of the imaging system was convolved with the original simulation results to yield the responses to the photon beam with a radius of 0.5 mm, the same as the size of the light beam used in the hyperspectral imaging system. The light intensity of the beam used in the imaging system was measured by a digital illumination meter (DX-200, INS Enterprise, Taipei, Taiwan), and the total power of the light beam was calculated using its lx value and the beam radius.

Absorption and reduced scattering coefficients are the most important input parameters for the Monte Carlo simulation model, and their values determine the major features of the simulation results. Four pairs of μ_a and μ_s' values, representing the minimum and maximum for the 600 apple fruit, were used as the input parameters to generate the typical results for spatially resolved diffuse reflectance that would cover all the apple samples. Since the simulation results directly depend on the values of μ_a and μ_s' but not on wavelength (Wang et al., 1995), it was not necessary to use the combinations of μ_a and μ_s' from the same wavelength. The actual values of μ_a and μ_s' used for the simulations are presented in Section 3.

Table 1
Input parameters for Monte Carlo simulation of light transport in fruit tissue.

Parameter	Value
Number of photons	3,000,000
Spatial resolution of radial distance (dr)	0.1 mm
Spatial resolution of tissue depth (dz)	0.1 mm
Number of grids for radial distance r	400
Number of grids for tissue depth z	400
Refractive index for medium above (air)	1.00
Refractive index for apple fruit tissue	1.35
Intensity of the light beam	44.3 lx
Radius of the light beam	0.5 mm
Total power of the light beam	0.174 mW

Other subordinate parameters for the MC simulation model are summarized in Table 1. The number of photons used in the MC model was determined from preliminary tests using different number of photons to minimize the noise level for the simulated results. Three million photons were found to be enough to generate consistent results, and more photons did not improve the quality of the simulation results. The refractive indices for the medium above the sample (i.e., air) and the fruit tissue were assumed to be 1.00 and 1.35 (Mourant et al., 1997), respectively. Given the parameters in Table 1, the Monte Carlo model could generate simulation results for diffuse reflectance and internal photon absorption covering 40 mm of radial distance (r) and depth (z) with a spatial resolution of 0.1 mm. The publicly available codes for Monte Carlo simulation known as 'MCML' and 'CONV' developed by Wang et al. (1995, 1997) were used for the simulation of light transport in apple fruit and the convolution for the finite-size light beam, respectively. The simulation programs were validated by comparing the simulated diffuse reflectance [$R(r)$] with the diffusion theory model as well as experimental profiles extracted from the hyperspectral image of a selected 'Golden Delicious' apple. The optical properties with high and low levels of the absorption coefficient for the selected apple were used as input parameters for the MC simulations and the diffusion model.

2.6. Estimation of light penetration depth in apples

Knowledge of light penetration depths is valuable because it could help us in designing an appropriate sensing configuration to collect optical information from the interior tissue of a food sample. Different methods of defining or measuring light penetration depths have been reported in literature. Based on the diffusion theory, light penetration depth (δ) may be defined as the traveled distance by which the light intensity level is reduced by a factor of $1/e$ (~37%), and it is computed as the reciprocal of the effective attenuation coefficient (μ_{eff}) (Wilson and Jacques, 1990):

$$\delta = \frac{1}{\mu_{eff}} = \frac{1}{\sqrt{3\mu_a(\mu_a + \mu_s')}} \quad (2)$$

Light intensity in the turbid media follows an exponential decrease with μ_{eff} as the decay constant (Fig. 4). Lammertyn et al. (2000) defined the light penetration depth as the fruit slice thickness at which diffuse reflectance spectra were significantly different from those of a slice of infinite thickness. Fraser et al. (2001) suggested the 1% light penetration depth, which is defined as the distance where the light intensity is reduced to 1%. The 1% light penetration depth can be calculated as $\delta \ln(1/1\%) \approx 4.6\delta$, as shown in Fig. 4. In this study, we report on values of the 1% light penetration depth for the apple samples. Both absorption and scattering properties (μ_a and μ_s') of apples are wavelength-dependent, therefore, light penetration depth is also dependent on wavelength.

Mean spectra of μ_a and μ_s' for all 600 'Golden Delicious' apples were used to calculate the mean penetration depth in apples using

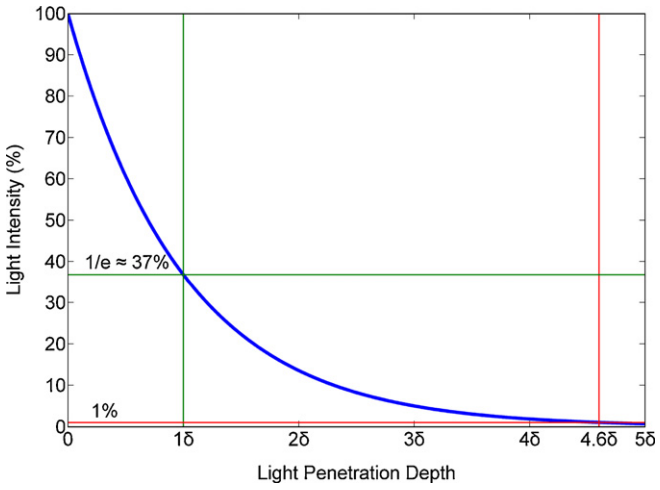

Fig. 4. Relationship between light attenuation in turbid media and light penetration depth. Light intensity follows an exponential decrease, and δ is the penetration depth by which light intensity level is reduced by a factor of $1/e$.

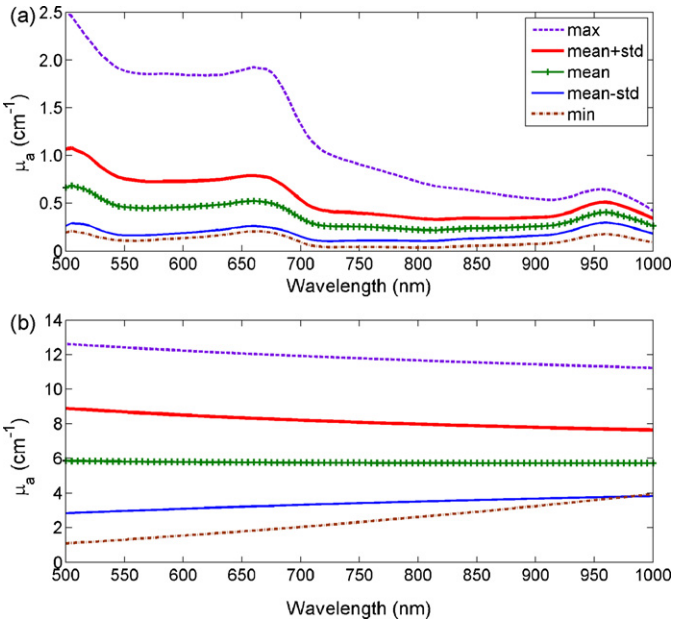

Fig. 5. Optical properties of 600 'Golden Delicious' apples: (a) absorption and (b) reduced scattering spectra.

Eq. (2). To further evaluate the range of light penetration depth in the apples within the visible and short-wave near-infrared region, the μ_a and μ_s' data of one standard deviation from their mean values as well as the minimum and maximum μ_a and μ_s' spectra were also used to calculate the penetration depth. Assuming both μ_a and μ_s' of the apples are normally distributed, one standard deviation from mean thus accounts for 68% of the entire data set. Consequently, the calculated penetration depth would cover approximately 68% of the apple data. The penetration depth calculated using minimum and maximum μ_a and μ_s' data represented the upper and lower limits for all 'Golden Delicious' apples.

3. Results and discussion

3.1. Optical properties of 'Golden Delicious' apples

Typical absorption and reduced scattering spectra, including mean, one standard deviation from mean, minimum, and maximum, for the 600 'Golden Delicious' apples over the spectral region of 500–1000 nm are presented in Fig. 5(a) and (b), respectively. The μ_a spectra of apples were peaked at 670 and 970 nm within the visible and short-wavelength near-infrared region, which were attributed to absorption by chlorophyll and water in the fruit tissue, respectively. For wavelengths from 730 to 900 nm, the absorption values were relatively small and stable. For the spectral range less than 550 nm, absorption due to carotenoid in the fruit tissue, which has an absorption peak at 480 nm (Merzlyak et al., 2003), became more evident. The minimum value of μ_a for all apple samples was 0.04 cm^{-1}, which appeared around 800 nm in the relatively flat absorption range of 730–900 nm. The maximum absorption (μ_a = 2.52 cm^{-1}) occurred at 500 nm, which corresponded to the absorption shoulder of the carotenoid.

Unlike the prominent 'fingerprints' appearing in the absorption spectra, the scattering spectra did not show particular spectral features. Most of the test 'Golden Delicious' apples showed a trend of steadily decreasing μ_s' values with the increase of wavelength, whereas the rest of the samples either exhibited a trend of increasing μ_s' values with the wavelength or remained nearly constant over the entire wavelength range. The μ_s' values for all the test samples were in a range from 1.02 to 12.61 cm^{-1}. The μ_s' values for approximately 68% of the apples (i.e., one standard deviation from the mean) ranged between 2.84 and 8.89 cm^{-1}. Overall the values of μ_s' were much greater than the μ_a values for the test samples, indicating the dominant effect of scattering in apples over the visible and short-wave near-infrared region.

3.2. Validation of Monte Carlo simulation

The optical properties of the selected apple at 670 and 800 nm, which represented the high and low levels of light absorption, respectively (see Fig. 5), were used in the MC simulations and the diffusion model for validating the simulation results. Fig. 6 shows experimental data and the validation results from Monte Carlo simulations and diffusion theory model. The spatial profiles from the simulation and the diffusion model as well as the experiment were not on the same scale. For the convenience of direct comparisons, all profiles were normalized at the initial point of the experimental data (1.6 mm to the source). The spatial profiles extracted from the hyperspectral image of the selected 'Golden Delicious' apple had been already calibrated for taking into account the effect of nonuniform instrument response and fruit size (Qin and Lu, 2008). Monte Carlo simulation results perfectly matched the diffusion theory model in the source-detector separations from 1.6 to 20.0 mm. The simulation results also agreed well with the experimental profiles at 670 and 800 nm, although the discrepancies beyond 10 mm

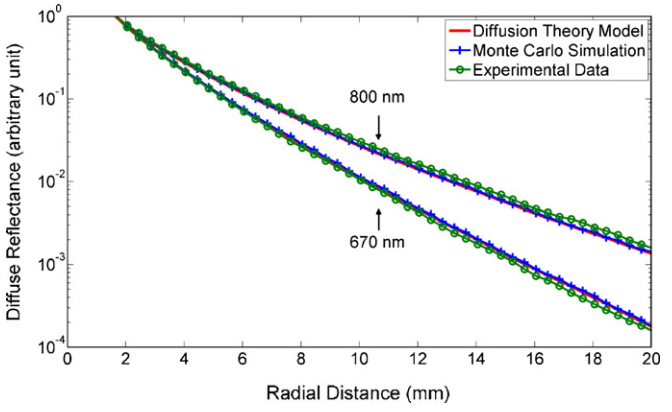

Fig. 6. Validation of Monte Carlo simulations for diffuse reflectance at 670 and 800 nm.

Table 2
Percent of incident photons partitioned into diffuse reflectance and internal absorption calculated by Monte Carlo simulations with the combinations of μ_a and μ'_s values for 'Golden Delicious' apples.

Combination	μ_a (cm^{-1})	μ'_s (cm^{-1})	Reflectance (%)	Absorption (%)
$\mu_{a\,max}$ and $\mu'_{s\,max}$	2.52	12.61	17.4	80.4
$\mu_{a\,max}$ and $\mu'_{s\,min}$	2.52	1.02	1.4	96.4
$\mu_{a\,min}$ and $\mu'_{s\,max}$	0.04	12.61	75.9	21.9
$\mu_{a\,min}$ and $\mu'_{s\,min}$	0.04	1.02	42.8	55.0

became larger than those at the near scattering distances. The validation results suggest that the Monte Carlo method can generate reliable simulation results for both high and low light absorption conditions.

3.3. Diffuse reflectance and internal absorption

In the Monte Carlo simulation of light transport in a medium with large thickness, no transmission through the material would be expected and all photon packets would eventually be separated into three components: specular reflectance, diffuse reflectance, and internal absorption. The refractive index of 'Golden Delicious' apples was assumed to be 1.35, thus the portion of specular reflectance from the fruit surface was calculated to be 2.2% using Fresnel equations. The remaining 97.8% of the photon weights were then transmitted into the fruit tissue, scoring into the diffuse reflectance and the internal absorption components, respectively. The fractions for diffuse reflectance and internal absorption for the given values of μ_a and μ'_s are summarized in Table 2.

The maximum of 96.4% for internal absorption was observed for the combination of $\mu_{a\,max}$ and $\mu'_{s\,min}$. The percent of internal absorption was reduced to 80.4% when μ'_s increased from the minimum to the maximum ($\mu_{a\,max}$ and $\mu'_{s\,max}$) while μ_a remained constant at the maximum. For the minimum absorption cases ($\mu_{a\,min}$ and $\mu'_{s\,max}$, and $\mu_{a\,min}$ and $\mu'_{s\,min}$), 75.9% and 42.8% photons exited from the sample surface as diffuse reflectance for maximum and minimum μ'_s values, respectively. The allocations of incident photons to diffuse reflectance and internal absorption are related to the ratio of μ'_s to μ_a or the transport albedo defined as $\mu'_s/(\mu_a + \mu'_s)$. A relatively large μ'_s value results in a large percent of diffuse reflectance. The same is also true for the relation of μ_a with internal absorption.

3.4. Simulation results for diffuse reflectance

Monte Carlo simulation results for the spatially resolved diffuse reflectance using four combinations of μ_a and μ'_s values including the minima and maxima are shown in Fig. 7. Patterns of the diffuse reflectance profiles are clearly determined by the values of μ_a and μ'_s. For the minimum absorption cases ($\mu_{a\,min}$ and $\mu'_{s\,max}$, and $\mu_{a\,min}$ and $\mu'_{s\,min}$), the attenuation rates of the spatial profiles were relatively flat towards the longer radial distances. The shapes of the two profiles were different due to the different values of μ'_s, and the combination of $\mu_{a\,min}$ and $\mu'_{s\,min}$ generated the minimum attenuation rate for the spatially resolved diffuse reflectance profiles. On the other hand, diffuse reflectance dropped dramatically for the maximum absorption cases ($\mu_{a\,max}$ and $\mu'_{s\,max}$, and $\mu_{a\,max}$ and $\mu'_{s\,min}$), and the maximum attenuation rate occurred when both μ_a and μ'_s were at their maximum values.

The spatial diffuse reflectance profiles presented in Fig. 7 were the convolved results, and they were linked to light source intensity through the convolution between the original simulation results from an infinitely narrow photon beam and the light source profile of the hyperspectral imaging system. Therefore, they can be used to find the optimum sensing range for 'Golden Delicious' apples. The optimum imaging range of the CCD camera used in

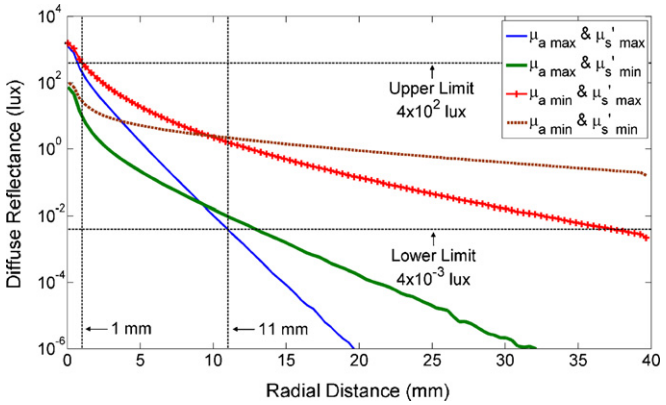

Fig. 7. Monte Carlo simulation results for diffuse reflectance obtained using different combinations of μ_a and μ'_s values for 'Golden Delicious' apples. See Table 2 for actual values of μ_a and μ'_s.

the imaging system was between 10^{-3} and 10^2 lx. The efficiency of the imaging spectrograph was greater than 50%, and the minimum transmission of the zoom lens in the visible and short-wavelength near-infrared region was approximately 50%. Before reaching the CCD camera, the diffusely reflected light passed through the zoom lens and the imaging spectrograph that had a combined transmission of approximately 25%, thus the optimum imaging range for diffuse reflectance from the fruit surface was estimated to be between 4×10^{-3} and 4×10^2 lx, as illustrated in Fig. 7. Corresponding to the upper and lower detection limits, the optimum sensing range under the current imaging system setup for 'Golden Delicious' apples would be in the radial range from 1 to 11 mm, as illustrated in Fig. 7. In this study, the spatial profiles covering 1.6–10 mm were used in the curve fitting procedures for determining the optical properties of the apples, which were within the optimum sensing range determined from the Monte Carlo simulations. The above discussion demonstrated that Monte Carlo simulations can aid in selecting or adjusting the sensing ranges for a given imaging system to achieve the optimal sensing configuration. Conversely, Monte Carlo simulations can assist in selecting an appropriate imaging system (i.e., light source, CCD camera and other optical components) when the sensing range and/or mode has been determined.

3.5. Simulation results for internal photon absorption

Fig. 8(a)–(d) presents Monte Carlo simulation results for the photon absorption power densities inside an apple using four combinations of μ_a and μ'_s values listed in Table 2. The results are shown as contour maps versus sample depth and radial distance, in which the values (i.e., 0.1, 0.01, and 0.001) marked on the contours of Fig. 8(a)–(d) represent the probability of the photon absorption by fruit tissue or the distributions of the deposited light energy inside the fruit tissue, expressed in the units of mW/cm^3. Similar to the diffuse reflectance profiles, the absorption density patterns in the fruit tissue were also greatly shaped by the combinations of μ_a and μ'_s values. The patterns of absorption in the fruit tissue were influenced by the value of μ_a, as shown in Fig. 8(a) and (c); fruit tissue with a large μ_a absorbs light energy rapidly in a relatively short depth and radial distance, and consequently it is more difficult for light to propagate into the deeper and broader areas. Comparing Fig. 8(a) and (b) shows that a larger μ'_s value also prevents light from penetrating the deeper area of the fruit tissue. Moreover, fruit tissue with a larger μ'_s value would broaden light in the radial (horizontal) direction, whereas the tissue with a small μ'_s value tended to propagate forward (vertical) into the deeper area of the sample. When μ'_s was at minimum, strong forward propagations along the direction of the incident light were observed (Fig. 8(b) and (d)). If

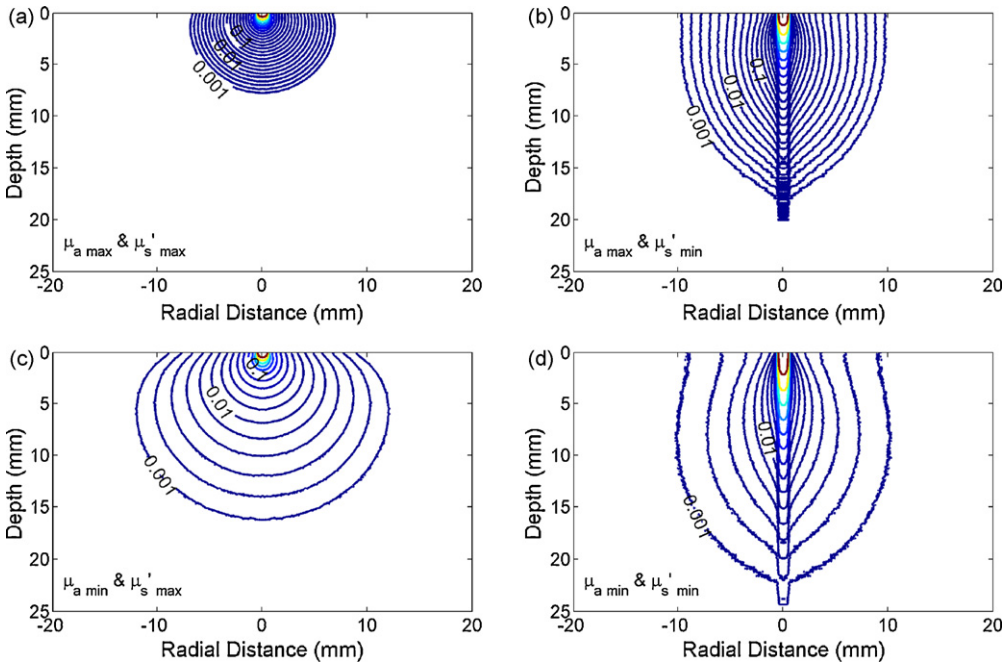

Fig. 8. Monte Carlo simulation results for photon absorption power densities (in mW/cm^3) inside a 'Golden Delicious' apple using different combinations of μ_a and μ'_s values: (a) $\mu_{a\,max}$ and $\mu'_{s\,max}$; (b) $\mu_{a\,max}$ and $\mu'_{s\,min}$; (c) $\mu_{a\,min}$ and $\mu'_{s\,max}$; (d) $\mu_{a\,min}$ and $\mu'_{s\,min}$. See Table 2 for actual values of μ_a and μ'_s.

there is no scattering at all (e.g., pure water), light will go straight without propagating into the lateral areas. Similar absorption pattern changes were observed in Fig. 8(b) and (d) as well as in Fig. 8(c) and (d).

Fig. 9(a) and (b) shows the absorption power density profiles versus the sample depth at $r=0$ and the radial distance at $z=0$ (see Fig. 3), respectively. The absorption power density in the fruit tissue generally decreased with the increase of depth and radial distance. Sudden power density drops were observed around the radial distance of 0.5 mm (Fig. 9(b)), indicating the dramatic internal absorption changes along the radial direction near the incident point. For both sample depth and radial distance, fruit tissues with $\mu_{a\,max}$ and $\mu'_{s\,max}$, and $\mu_{a\,min}$ and $\mu'_{s\,min}$ had the maximum and minimum attenuation rates of absorption density, respectively, and the other two tissues possessed some intermediate attenuation rates. The patterns of the profiles plotted in Fig. 9(a) and (b) confirmed the findings from Fig. 8(a)–(d) described above.

3.6. Light penetration depth in apples

The calculated 1% light penetration depths in 'Golden Delicious' apples, which include mean, one standard deviation from mean, and the upper and lower limits, are shown in Fig. 10. A minimum penetration depth of 0.43 cm was observed at the wavelength of 500 nm, which is the spectral position where both light absorption and scattering were strong (see Fig. 5). The penetration depths at the absorption peaks of chlorophyll and water (i.e., 670 and 970 nm) appeared as local minima. The maximum penetration depth, which was 8.67 cm, was located around 725 nm in the flat region of the absorption spectra (see Fig. 5). Over the spectral region from 500 to 1000 nm, the mean light penetration depth varies between 1.26 and 2.33 cm with an average value of 1.86 cm. The penetration depths for one standard deviation from mean, which accounted for 68% of all 600 'Golden Delicious' apples, were in the range of 0.81–4.48 cm.

Light penetration depth is directly related to light attenuation in the fruit tissue, which involves both absorption and scattering. Pigments and water are strong absorbing constituents in the fruit tissue, and they determine the major spectral features of light

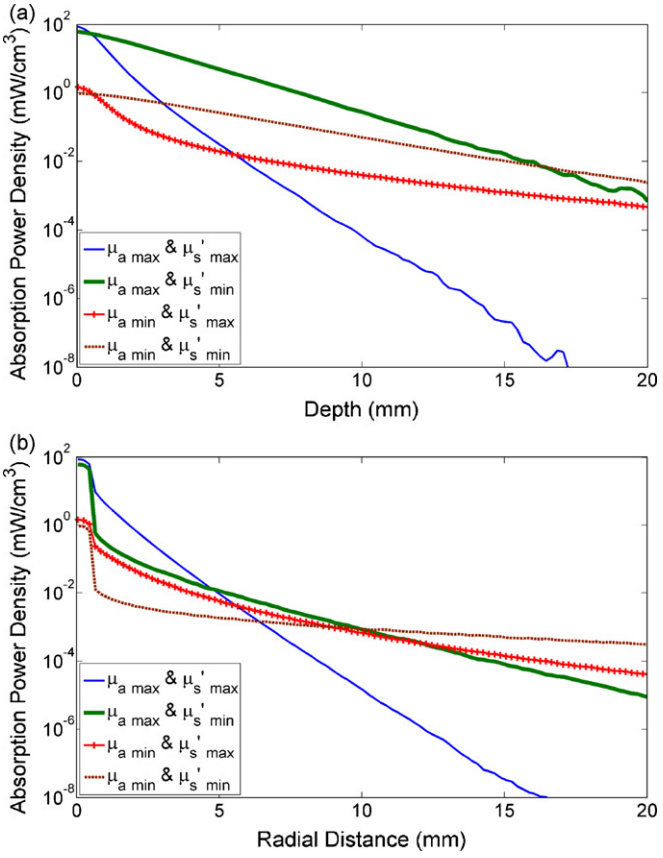

Fig. 9. Monte Carlo simulation results for internal photon absorption power densities versus (a) depth and (b) radial distance. See Table 2 for actual values of μ_a and μ'_s.

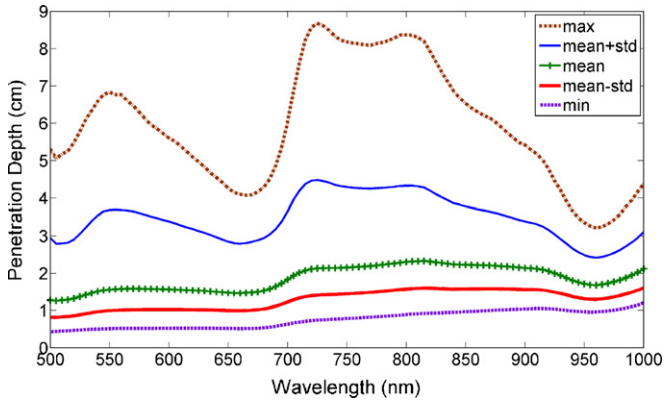

Fig. 10. Light penetration depth in 'Golden Delicious' apples.

penetration in apples, although scattering properties are also indispensable for determining the absolute values of penetration depth. The overall patterns of light penetration depth in 'Golden Delicious' apples obtained in this study are consistent with those for 'Jonagold' apples measured using an experimental method via an optical fiber probe (Lammertyn et al., 2000). The penetration depth in 'Golden Delicious' apples calculated from Eq. (2) was larger than that in 'Jonagold' apples (0.2–0.4 cm). Fraser et al. (2001) reported penetration depths (e.g., 3.5 cm at 713 nm) that are comparable with those obtained in this study. Different results should have been expected since the definition of light penetration depth, instrument performance/setup, and fruit variety and condition were different in the current and other studies.

4. Summary and conclusions

The absorption and reduced scattering coefficients of 'Golden Delicious' apples were determined over the spectral range of 500–1000 nm using a spatially resolved hyperspectral diffuse reflectance imaging technique, and they were used as input parameters for Monte Carlo models to simulate light transport features in apple fruit. Monte Carlo simulation models were validated by diffusion theory model and experimental data. The major features of light transport in apples were determined using Monte Carlo simulations. The patterns of diffuse reflectance, internal absorption, and light penetration depth were all shaped by the combination of μ_a and μ_s' values. Fruit tissue with a larger μ_a value absorbed light energy rapidly in a relatively short depth and radial distance, and light in the tissue with a small μ_s' value tended to propagate forward to the deeper area of the sample. Light penetration depth in 'Golden Delicious' apples ranged from 0.43 to 8.67 cm for the wavelength range of 500–1000 nm, and strong absorbing constituents in fruit tissue (i.e., pigments and water) determined major spectral features of the penetration depth. The simulated diffuse reflectance profiles can be used to find the optimum sensing range for apple samples, and they are also useful for determining or adjusting operation ranges for individual imaging system components such as light source and camera to achieve the best sensing conditions.

References

Arridge, S.R., Schweiger, M., Hiraoka, M., Delpy, D.T., 1993. A finite-element approach for modeling photon transport in tissue. Med. Phys. 20, 299–309.
Bass, M., Van Stryland, E., Williams, D., Wolfe, W. (Eds.), 1995. Handbook of Optics. McGraw-Hill, New York, NY, USA.
Cubeddu, R., D'Andrea, C., Pifferi, A., Taroni, P., Torricelli, A., Valentini, G., Dover, C., Johnson, D., Ruiz-Altisent, M., Valero, C., 2001. Nondestructive quantification of chemical and physical properties of fruits by time-resolved reflectance spectroscopy in the wavelength range 650–1000 nm. Appl. Opt. 40, 538–543.
Deulin, X., L'Huillier, J.P., 2006. Finite element approach to photon propagation modeling in semi-infinite homogeneous and multilayered tissue structures. Eur. Phys. J. Appl. Phys. 33, 133–146.
Farrell, T.J., Patterson, M.S., Wilson, B., 1992. A diffusion-theory model of spatially resolved, steady-state diffuse reflectance for the noninvasive determination of tissue optical-properties in vivo. Med. Phys. 19, 879–888.
Fraser, D.G., Künnemeyer, R., McGlone, V.A., Jordan, R.B., 2001. Near infra-red (NIR) light penetration into an apple. Postharvest Biol. Technol. 22, 191–194.
Fraser, D.G., Jordan, R.B., Künnemeyer, R., McGlone, V.A., 2003. Light distribution inside mandarin fruit during internal quality assessment by NIR spectroscopy. Postharvest Biol. Technol. 27, 185–196.
Ishimaru, A., 1978. Wave Propagation and Scattering in Random Media. Academic Press, New York, NY, USA.
Kienle, A., Lilge, L., Patterson, M.S., Hibst, R., Steiner, R., Wilson, B.C., 1996. Spatially resolved absolute diffuse reflectance measurements for noninvasive determination of the optical scattering and absorption coefficients of biological tissue. Appl. Opt. 35, 2304–2314.
Lammertyn, J., Peirs, A., De Baerdemaeker, J., Nicolai, B., 2000. Light penetration properties of NIR radiation in fruit with respect to non-destructive quality assessment. Postharvest Biol. Technol. 18, 121–132.
Lu, R., Chen, Y.R., 1998. Hyperspectral imaging for safety inspection of food and agricultural products. In: Proceedings of SPIE 3544. SPIE, Willmington, WA, pp. 121–133.
Merzlyak, M.N., Solovchenko, A.E., Gitelson, A.A., 2003. Reflectance spectral features and non-destructive estimation of chlorophyll, carotenoid and anthocyanin content in apple fruit. Postharvest Biol. Technol. 27, 197–211.
Mourant, J.R., Fuselier, T., Boyer, J., Johnson, T.M., Bigio, I.J., 1997. Predictions and measurements of scattering and absorption over broad wavelength ranges in tissue phantoms. Appl. Opt. 36, 949–957.
Okada, E., Firbank, M., Schweiger, M., Arridge, S.R., Cope, M., Delpy, D.T., 1997. Theoretical and experimental investigation of near-infrared light propagation in a model of the adult head. Appl. Opt. 36, 21–31.
Palmer, G.M., Ramanujam, N., 2006. Monte Carlo-based inverse model for calculating tissue optical properties. Part I: Theory and validation on synthetic phantoms. Appl. Opt. 45, 1062–1071.
Qin, J., Lu, R., 2007. Measurement of the absorption and scattering properties of turbid liquid foods using hyperspectral imaging. Appl. Spectrosc. 61, 388–396.
Qin, J., Lu, R., 2008. Measurement of the optical properties of fruits and vegetables using spatially resolved hyperspectral diffuse reflectance imaging technique. Postharvest Biol. Technol. 49, 355–365.
Saeys, W., Velazco-Roa, M.A., Thennadil, S.N., Ramon, H., Nicolaï, B.M., 2008. Optical properties of apple skin and flesh in the wavelength range from 350 to 2200 nm. Appl. Opt. 47, 908–919.
Simpson, C.R., Kohl, M., Essenpreis, M., Cope, M., 1998. Near-infrared optical properties of ex vivo human skin and subcutaneous tissues measured using the Monte Carlo inversion technique. Phys. Med. Biol. 43, 2465–2478.
Tsai, C.L., Yang, Y.F., Han, C.C., Hsieh, J.H., Chang, M., 2001. Measurement and simulation of light distribution in biological tissues. Appl. Opt. 40, 5770–5777.
Wang, L.H., Jacques, S.L., Zheng, L.Q., 1995. MCML—Monte-Carlo modeling of light transport in multilayered tissues. Comput. Methods Programs Biol. 47, 131–146.
Wang, L.H., Jacques, S.L., Zheng, L.Q., 1997. CONV—convolution for responses to a finite diameter photon beam incident on multi-layered tissues. Comput. Methods Programs Biol. 54, 141–150.
Wang, L.H., Liang, G., 1999. Absorption distribution of an optical beam focused into a turbid medium. Appl. Opt. 38, 4951–4958.
Wilson, B.C., Jacques, S.L., 1990. Optical reflectance and transmittance of tissues: principles and applications. IEEE J. Quantum Electron. 26, 2186–2199.